Sliding Mode Control of a Three Degrees of Freedom Anthropoid Robot by Driving the Controller Parameters to an Equivalent Regime

M. Onder Efe
e-mail: efemond@boun.edu.tr

Okyay Kaynak
e-mail: kaynak@boun.edu.tr

Electrical and Electronic Engineering
Department, Bogazici University,
Bebek, 80815, Istanbul, Turkey

Xinghuo Yu
Faculty of Informatics and Communication,
Central Queensland University
Rockhampton QLD 4702, Australia
e-mail: X.Yu@cqu.edu.au

Noise rejection, handling the difficulties coming from the mathematical representation of the system under investigation and alleviation of structural or unstructural uncertainties constitute prime challenges that are frequently encountered in the practice of systems and control engineering. Designing a controller has primarily the aim of achieving the tracking precision as well as a degree of robustness against the difficulties stated. From this point of view, variable structure systems theory offer well formulated solutions to such ill-posed problems containing uncertainty and imprecision. In this paper, a simple controller structure is discussed. The architecture is known as Adaptive Linear Element (ADALINE) in the framework of neural computing. The parameters of the controller evolve dynamically in time such that a sliding motion is obtained. The inner sliding motion concerns the establishment of a sliding mode in controller parameters, which aims to minimize the error on the controller outputs. The outer sliding motion is designed for the plant. The algorithm discussed drives the error on the output of the controller toward zero learning error level, and the state tracking error vector of the plant is driven toward the origin of the phase space simultaneously. The paper gives the analysis of the equivalence between the two sliding motions and demonstrates the performance of the algorithm on a three degrees of freedom, anthropoid robotic manipulator. In order to clarify the performance of the scheme, together with the dynamic complexity of the plant, the adverse effects of observation noise and nonzero initial conditions are studied.
[S0022-0434(00)01704-4]

Keywords: Sliding Mode Control, Adaptive Control, ADALINE, Robotics, Dynamic Adaptation

1 Introduction

It is a well-known fact that a variable structure controller with a switching output will (under certain circumstances) result in a sliding mode on a predefined subspace of the state space. This mode has useful invariance properties in the face of uncertainties in the plant model and therefore is a candidate for tracking control of uncertain nonlinear systems. The theory is well developed, especially for single input systems in controller canonical form. The philosophy of the control strategy is simple, being based on two goals. First, the system is forced toward a desired dynamics, second, the system is maintained on that differential geometry. In the literature, the former dynamics is named the reaching mode, while the latter is called the sliding mode. The control strategy borrows its name from the latter dynamic behavior, and is called *Sliding Mode Control (SMC)*.

Earliest notion of SMC strategy was constructed on a second-order system in the late 1960s by Emelyanov [1]. The work stipulated that a special line could be defined on the phase plane, such that any initial state vector can be driven toward the plane and then be maintained on it, while forcing the error dynamics toward the origin. Since then, the theory has been greatly improved and the sliding line has taken the form of a multidimensional surface, called the *sliding surface* around which a switching control action takes place.

In Variable Structure Control (VSC), the existence of observation noise constitutes a prime difficulty. This is due to the fact that the pure sliding control requires very fast switching on the input, which cannot be provided by real actuators, and the input depends on the sign of a measured variable, which is very close to zero. This makes the control signal extremely vulnerable to measurement noise and may lead to unnecessarily large control signals. To alleviate these difficulties, several modifications to the original sliding mode control law have been proposed in the literature, some recent ones of which are based on the use of fuzzy logic [2–3] and artificial neural networks [4–5]. These methodologies provide an extensive freedom for control engineers to exploit their understanding of the problem, to deal with problems of uncertainty and imprecision.

During the last decade, numerous contributions to VSS theory have been made. Some of them are as follows. Hung et al. [6] has reviewed the control strategy for linear and nonlinear systems. In [6], the switching schemes, putting the differential equations into canonical forms and generating simple SMC strategies are considered in detail. In [7] and [8], applications of SMC scheme to robotic manipulators are studied and the quality of the scheme is discussed from the point of robustness. One of the crucial points in SMC is the selection of the parameters of the sliding surface. Some studies devoted to the adaptive design of sliding surfaces have shown that the performance of control system can be refined

Contributed by the Dynamic Systems and Control Division for publication in the JOURNAL OF DYNAMIC SYSTEMS, MEASUREMENT, AND CONTROL. Manuscript received by the Dynamic Systems and Control Division February 11, 2000. Associate Technical Editors: E. Misawa and V. Utkin.

by interfacing it with an adaptation mechanism, which regularly redesigns the sliding surface [8–9]. This eventually results in a robust control system. The performance of SMC scheme is proven to be satisfactory in the face of external disturbances and uncertainties in the system model representation. Another systematic examination of SMC approach is presented in [10]. In this reference, the practical aspects of SMC design are assessed for both continuous time and discrete time cases and a special consideration is given to the finite switching frequency, limited bandwidth actuators and parasitic dynamics, all leading to what is known as *chattering*. In [11], the design of discrete time SMC is presented with particular emphasis on the system model uncertainties. In [12–14], it is demonstrated that SMC strategy can be used for stabilization and robustification of learning dynamics of computationally intelligent methods. The approach presented in these references is based on the development of a dynamic model for the learning strategy and the design of a sliding motion in the parametric displacement space. The method studied in [12–14] has been applied to several neural network and fuzzy inference system models used for the purpose of controlling robotic manipulators.

Some studies on the use of SMC strategy are devoted to the dynamic adaptation of the parameters of a flexible model such that the error on the output of the model tends to zero in finite time [15–16]. The first results discussed by Ramirez et al. [15] have concentrated on the inverse dynamics identification of a Kapitsa pendulum by assuming constant bounds for uncertainties. Yu et al. [16] extend the results of [15] by introducing adaptive uncertainty bound dynamics and focus on the same example as the application. The major drawback in both of the approaches is the fact that the dynamic adaptation mechanism needs the error on the output of the model. If the model is to be used as a controller, this fact constitutes a difficulty because the use of the approaches proposed in [15–16] for control applications require the error on the control signal to be applied, which is unavailable. The second drawback of the dynamic uncertainty bound adaptation strategy in [16] is the existence of noise on the measured variables. The approach in [16] requires the integration of the absolute value of the error signal observed on the outputs. When the error signal is close to zero, it clearly leads to the integration of the absolute value of the noise signal, which gradually increases the bound value and leads to instability in the long run.

In this paper, existence of a relation between sliding surface for the plant to be controlled and the zero learning error level of the parameters of a flexible controller is discussed and the control applications of the method considered in [15–16] are studied with constant uncertainty bounds.

This paper is organized as follows: Section 2 gives the definitions and the formulation of the problem. Section 3 introduces the equivalency constraints on the sliding control performance for the plant and sliding mode learning performance for the controller. Section 4 describes the plant model used in the simulations. The section is followed by the simulation studies. Conclusions constitute the last part of the paper.

2 Definitions and the Formulation of the Problem

Consider the three input one output flexible structure, which is to be used as the controller, depicted in Fig. 1. The adjustable parameter vector and the input vector of the structure are described in (1) and (2), respectively. In (2), the symbol e denotes the tracking error, which is the discrepancy between the response of the system under control and the reference signal ($e=q-q_d$). The input output relation of the controller is described by (3).

$$G=[G_p \;\; G_d \;\; G_c]^T \tag{1}$$

$$u=[e \;\; \dot{e} \;\; 1]^T \tag{2}$$

$$\tau=G^T u \tag{3}$$

or equivalently,

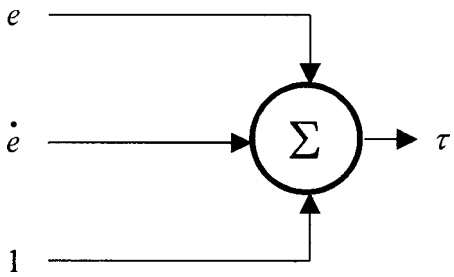

Fig. 1 Structure of the ADALINE controller

$$\tau=G_p e+G_d \dot{e}+G_c \tag{4}$$

The structure is assumed to operate in an ordinary feedback loop as illustrated in Fig. 2. The definitions of the sliding surface $s_p(e,\dot{e})$ and that of zero learning error level $s_c(\tau,\tau_d)$, which are seen in this figure, are given in (5) and (6), respectively.

$$s_p(e,\dot{e})=\dot{e}+\lambda e \tag{5}$$

where, λ is the slope of the sliding surface.

$$s_c(\tau,\tau_d)=\tau-\tau_d \tag{6}$$

where, τ_d is the desired output of the controller and is unknown.

In order not to be in conflict with the physical reality, the designer must impose the following inequalities, the truth of which state that the parameters of the controller, the time derivative of the input signal, and the time derivative of the desired output of the controller remain bounded.

$$\|G\|\leqslant B_G \tag{7}$$

$$\|\dot{u}\|\leqslant B_{\dot{u}} \tag{8}$$

$$\|\dot{\tau}_d\|\leqslant B_{\dot{\tau}_d} \tag{9}$$

Theorem 2.1. The adaptation of controller parameters as described in (10) enforces the parameters to values resulting in zero learning error level in one-dimensional phase space, whose argument is defined by (6).

$$\dot{G}=-\frac{u}{u^T u}k\,\mathrm{sign}(s_c) \tag{10}$$

where, k is a sufficiently large positive constant satisfying (11).

$$k>B_G B_{\dot{u}}+B_{\dot{\tau}_d} \tag{11}$$

The adaptation mechanism in (10) drives an arbitrary initial value of s_c to zero in finite time denoted by t_h satisfying the inequality in (12).

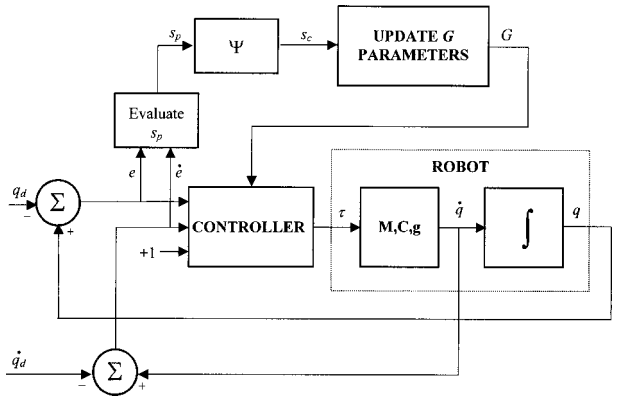

Fig. 2 Architecture of the control system

$$t_h \leq \frac{|s_c(0)|}{k-(B_G B_{\dot{u}}+B_{\dot{\tau}_d})} \tag{12}$$

Proof 2.1. Consider the Lyapunov function candidate in (13). In order to reach to the zero learning error level ($s_c=0$), the time derivative of (13) must be negative definite, which is given in (14).

$$V_c=\frac{1}{2}s_c^2 \tag{13}$$

$$\begin{aligned}\dot{V}_c &= \dot{s}_c s_c \\ &= (\dot{\tau}-\dot{\tau}_d)s_c \\ &= (\dot{G}^T u+G^T\dot{u}-\dot{\tau}_d)s_c \\ &= -k\,\mathrm{sign}(s_c)s_c+(G^T\dot{u}-\dot{\tau}_d)s_c \\ &= -k|s_c|+(G^T\dot{u}-\dot{\tau}_d)s_c \\ &< (-k+B_G B_{\dot{u}}+B_{\dot{\tau}_d})|s_c| \end{aligned} \tag{14}$$

It is apparent that the condition in (11) ensures the negative definiteness of the time derivative of the selected Lyapunov function.

If one evaluates $\dot{s}_c$ with the aid of (10), the expression in (15) is obtained. The solution to the differential equation in (15) can be given by (16).

$$\dot{s}_c=-k\,\mathrm{sign}(s_c)+G^T\dot{u}-\dot{\tau}_d \tag{15}$$

$$s_c(t)-s_c(0)=-kt\,\mathrm{sign}(s_c(0))+\int_0^t (G^T(\sigma)\dot{u}(\sigma)-\dot{\tau}_d(\sigma))d\sigma \tag{16}$$

At $t=t_h$, $s_c(t_h)=0$;

$$-s_c(0)=-kt_h\,\mathrm{sign}(s_c(0))+\int_0^{t_h} (G^T(\sigma)\dot{u}(\sigma)-\dot{\tau}_d(\sigma))d\sigma \tag{17}$$

By multiplying both sides of (17) by $-\mathrm{sign}(s_c(0))$, one obtains (18).

$$\begin{aligned}|s_c(0)| &= kt_h-\left(\int_0^{t_h}(G^T(\sigma)\dot{u}(\sigma)-\dot{\tau}_d(\sigma))d\sigma\right)\mathrm{sign}(s_c(0)) \\ &\geq kt_h-(B_G B_{\dot{u}}+B_{\dot{\tau}_d})t_h\end{aligned} \tag{18}$$

which implies hitting in finite time as described by the inequality in (12). □

Theorem 2.2. If the system enters the sliding mode $s_c=0$ and remains in it thereafter, then the parameters of the flexible controller, G, evolve boundedly.

Proof 2.2. In the sliding mode, $s_c=0$ and $\dot{s}_c=0$. Based on this, the following derivation can be made.

$$\dot{s}_c=\dot{\tau}-\dot{\tau}_d \tag{19}$$

$$\dot{s}_c=\dot{G}^T u+G^T\dot{u}-\dot{\tau}_d=0 \tag{20}$$

$$\begin{aligned}u^T\dot{G} &= -\dot{u}^T G+\dot{\tau}_d \\ &= -\frac{u^T u}{u^T u}\dot{u}^T G+\frac{u^T u}{u^T u}\dot{\tau}_d \\ &= u^T\left(-\frac{u}{u^T u}\dot{u}^T G+\frac{u}{u^T u}\dot{\tau}_d\right)\end{aligned} \tag{21}$$

which requires the following,

$$u^T\left(\dot{G}+\frac{u}{u^T u}\dot{u}^T G-\frac{u}{u^T u}\dot{\tau}_d\right)=0 \tag{22}$$

Since the entries of the vector u cannot be linearly dependent for all time [17], the equality in (22) imposes the following differential equation form in the sliding mode.

$$\dot{G}=-\frac{u\dot{u}^T}{u^T u}G+\frac{u}{u^T u}\dot{\tau}_d \tag{23}$$

The solution to the above equation is as follows;

$$G(t)=\Phi(t,0)G(0)+\int_0^t \Phi(t,\sigma)\frac{u(\sigma)}{u(\sigma)^T u(\sigma)}\dot{\tau}_d(\sigma)d\sigma \tag{24}$$

where,

$$\Phi(t,0)=\exp\left\{-\int_0^t \frac{u(\sigma)\dot{u}(\sigma)^T}{u(\sigma)^T u(\sigma)}d\sigma\right\} \tag{25}$$

Since $1\leq\|u\|\leq B_u$, for the first term in (24), following relations can be induced.

$$\begin{aligned}\|\Phi(t,0)\| &= \left\|\exp\left\{-\int_0^t \frac{u(\sigma)\dot{u}(\sigma)^T}{u(\sigma)^T u(\sigma)}d\sigma\right\}\right\| \\ &= \left\|\exp\left\{-\int_0^t \frac{u(\sigma)}{u(\sigma)^T u(\sigma)}du(\sigma)^T\right\}\right\| \\ &\leq \left\|\exp\left\{\left|-\int_0^t \frac{u(\sigma)}{u(\sigma)^T u(\sigma)}du(\sigma)^T\right|\right\}\right\| \\ &\leq \left\|\exp\left\{\int_0^t \frac{|u(\sigma)|}{u(\sigma)^T u(\sigma)}du(\sigma)^T\right\}\right\| \\ &< \left\|\exp\left\{\int_0^t |u(\sigma)|du(\sigma)^T\right\}\right\| \\ &< \left\|\exp\left\{B_u\int_0^t du(\sigma)^T\right\}\right\| \\ &= \|\exp\{B_u(u(t)^T-u(0)^T)\}\|\leq B_1\end{aligned} \tag{26}$$

where B_1 is some positive constant. For the bound of the second term in (24), the analysis proceeds as given below.

$$\begin{aligned}&\left\|\int_0^t \Phi(t,\sigma)\frac{u(\sigma)}{u(\sigma)^T u(\sigma)}\dot{\tau}_d(\sigma)d\sigma\right\| \\ &< B_1\left\|\int_0^t \frac{u(\sigma)}{u(\sigma)^T u(\sigma)}\dot{\tau}_d(\sigma)d\sigma\right\| \\ &< B_1\left\|\int_0^t u(\sigma)\dot{\tau}_d(\sigma)d\sigma\right\| \\ &< B_1 B_u\left\|\int_0^t \dot{\tau}_d(\sigma)d\sigma\right\| \\ &< B_1 B_u\|\tau_d(t)-\tau_d(0)\|\leq B_2\end{aligned} \tag{27}$$

where B_2 is some positive constant. Since the two components of the solution in (24) evolve boundedly, the sum of them will trivially be bounded as given in (28).

$$\|G(t)\|<B_1+B_2 \tag{28}$$

□

Note that in (7) we assumed that the parameters of the flexible controller, G, are bounded. However, Theorem 2.2 states that once the system enters the sliding mode $s_c=0$, the boundedness of G is guaranteed. That is to say that (7) is automatically satisfied.

In the view of the analysis presented, the parameters of the controller are adjusted as described explicitly in (29)–(31).

$$\dot{G}_p = -\frac{e}{e^2+\dot{e}^2+1}k\,\mathrm{sign}(s_c) \tag{29}$$

$$\dot{G}_d = -\frac{\dot{e}}{e^2+\dot{e}^2+1}k\,\mathrm{sign}(s_c) \tag{30}$$

$$\dot{G}_c = -\frac{1}{e^2+\dot{e}^2+1}k\,\mathrm{sign}(s_c) \tag{31}$$

The main problem in applying the design presented is the unavailability of the desired value of the control signal (τ_d). If this quantity is not available, one cannot construct s_c and the approach cannot be used for control purposes. In the next section, the relation between the s_p of (5) and s_c of (6) is analyzed.

3 Analysis of the Relation Between Sliding Mode Control and Sliding Mode Learning

Consider the sliding line s_p and the zero learning error level s_c described by (5) and (6), respectively. In the most general sense, the relation between these two quantities can be written as in (32), in which the integers n and m characterize the differential relation between s_p and s_c and the values of which are quite difficult to obtain if the system dynamics is uncertain. Assume that $m=n=0$; qualitatively, if the value of s_p tends to zero, this means that s_c goes to zero. Physically, the system achieves a perfect tracking because the controller produces the desired control inputs or vice versa. Conversely, as the value of s_p increases in magnitude, which means that the error vector is getting away from the origin, the same sort of a divergent behavior in s_c is observed or vice versa. In this section, three conditions that Ψ must satisfy are discussed.

$$s_c^{(n)} = \Psi(s_p^{(m)}) \tag{32}$$

3.1 Region Condition. It should be clear that as the control input approaches to the desired control value for the current conditions, this means that the state tracking error vector of the plant is driven toward the sliding manifold. In other words, the desired control signal drives the state tracking error to the sliding manifold. In (33), these two statements are clarified.

$$\lim_{\tau\to\tau_d} s_p = 0 \Leftrightarrow \lim_{s_p\to 0} \tau = \tau_d \tag{33}$$

The two equivalent limits and their consequences can be rewritten as given in (34) and (35) by utilizing s_p and s_c.

$$\lim_{s_c\to 0} s_p = 0 \Rightarrow \left\{ \dot{e}\to -\lambda e \Rightarrow \begin{cases} e\to 0 \\ \dot{e}\to 0 \end{cases} \right. \tag{34}$$

$$\lim_{s_p\to 0} s_c = 0 \Rightarrow \{\tau\to\tau_d \tag{35}$$

The statements above require the following condition on Ψ.

$$\Psi(0) = 0 \tag{36}$$

Furthermore, as indicated in Fig. 3, the relation Ψ must use the first and the third quadrants of the coordinate system.

$$\Psi(x) = \begin{cases} \text{positive} & x>0 \\ \text{zero} & x=0 \\ \text{negative} & x<0 \end{cases} \tag{37}$$

3.2 Compatibility Condition. In order to measure the tracking performance of the control system; define the Lyapunov function in (38). The realization performance of the controller (V_c) has already been defined in (13). In Fig. 4, two sets are illustrated. If one selects a Ψ relation such that a simultaneous minimization is achieved, then this selection can be considered as a suitable candidate. Since Ψ candidates from the regions other than the shaded set causes the violation of at least one of the design objectives, one has to find a Ψ relation from the intersection set.

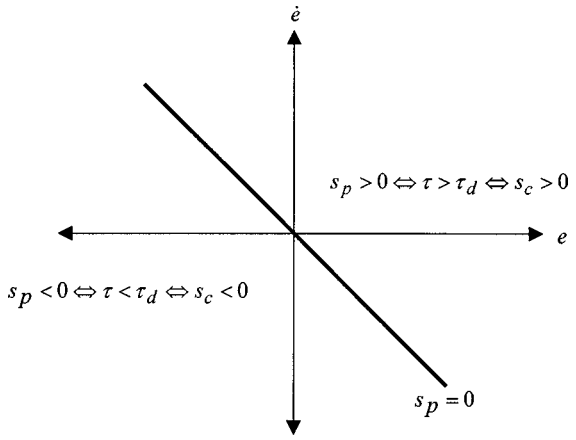

Fig. 3 Signs of s_p and s_c on different sides of $s_p=0$ line

$$V_p = \frac{1}{2}s_p^2 \tag{38}$$

3.3 Invertibility Condition. As depicted in Fig. 5, if the family of lines described by $s_p=\eta$ ($\eta>0$) are drawn for varying values of η, the tracking error vector will fall into one of these subsets of the phase space at each instant of time. However, each one of the members of this family corresponds to a different situation entailing different s_c values. Therefore the relation Ψ must be invertible. In other words, $\exists s_p\in\Re$ for $\forall s_c\in\Re$.

These three conditions clearly stipulate that the Ψ relation must be such that the horizontal axes of the two subplots shown in Fig. 6 must be mapped onto each other for simultaneous minimization of the shown quadratic functions.

Theorem 3.1. All monotonically increasing continuous functions can serve as the Ψ relation, which satisfy the three conditions discussed in Section 3.1–Section 3.3, for the establishment of an equivalency between the sliding mode control of the plant and the sliding mode learning inside the controller.

Proof 3.1. Stability in the Lyapunov sense requires the negative definiteness of the time derivative of the Lyapunov function in (38). Utilizing (39) leads to the following time derivative.

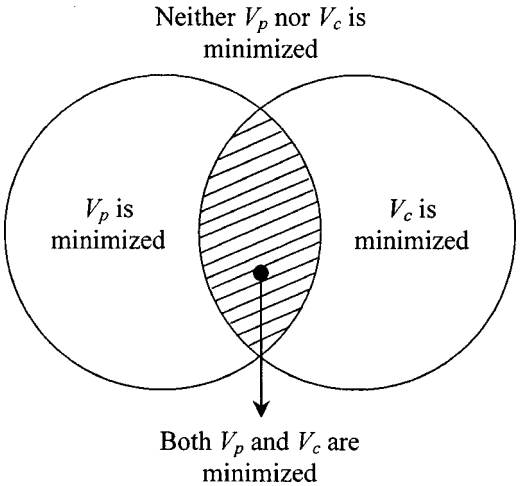

Fig. 4 Sets of possible four cases

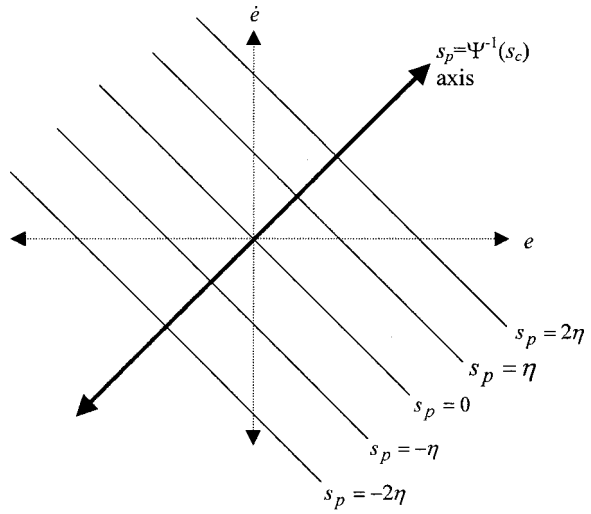

Fig. 5 The family of lines formed as the value of s_p varies

$$s_p=\Psi^{-1}(s_c) \tag{39}$$

$$\begin{aligned}
\dot{V}_p &= \dot{s}_p s_p \\
&= \dot{(}\Psi^{-1}(s_c))\Psi^{-1}(s_c) \\
&= \frac{\partial\Psi^{-1}(s_c)}{\partial s_c}\dot{s}_c\Psi^{-1}(s_c) \\
&= \frac{\partial\Psi^{-1}(s_c)}{\partial s_c}(\dot{G}^T u+G^T\dot{u}-\dot{\tau}_d)\Psi^{-1}(s_c) \\
&= \frac{\partial\Psi^{-1}(s_c)}{\partial s_c}(-k\,\mathrm{sign}(s_c)+G^T\dot{u}-\dot{\tau}_d)\Psi^{-1}(s_c) \\
&= \frac{\partial\Psi^{-1}(s_c)}{\partial s_c}(\Psi^{-1}(s_c)(G^T\dot{u}-\dot{\tau}_d)-k(\Psi^{-1}(s_c)\mathrm{sign}(s_c))) \\
&\leqslant \frac{\partial\Psi^{-1}(s_c)}{\partial s_c}(|\Psi^{-1}(s_c)|(B_G B_{\dot{u}}+B_{\dot{\tau}_d})-k(\Psi^{-1}(s_c)\mathrm{sign}(s_c))) \\
&= \frac{\partial\Psi^{-1}(s_c)}{\partial s_c}(|\Psi^{-1}(s_c)|(B_G B_{\dot{u}}+B_{\dot{\tau}_d})-k|\Psi^{-1}(s_c)|) \\
&= \frac{\partial\Psi^{-1}(s_c)}{\partial s_c}|\Psi^{-1}(s_c)|(-k+B_G B_{\dot{u}}+B_{\dot{\tau}_d})
\end{aligned} \tag{40}$$

Since the partial derivative $\partial\Psi^{-1}(s_c)/\partial s_c$ is positive due to the monotonically increasing behavior of Ψ, the bound parameter given in (11) enforces value of s_c to zero level, or equivalently, s_p to zero. It is straightforward to prove that a hitting occurs in finite time (see Proof 2.1). □

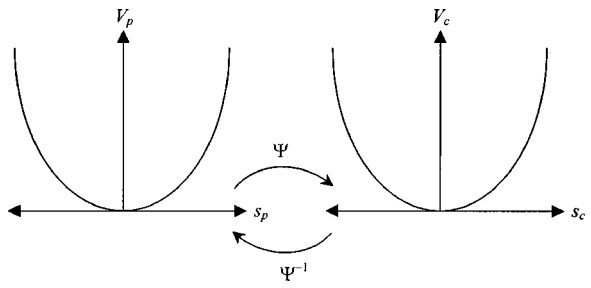

Fig. 6 The relation Ψ performs a mapping between two horizontal axes shown

4 A 3-DOF Anthropoid Robot Dynamics

In this study, the dynamic model of the three degrees of freedom anthropoid robotic manipulator, whose physical structure is illustrated in Fig. 7, is used as the test bed. Since the dynamics of such a mechatronic system is modeled by nonlinear and coupled differential equations, precise output tracking becomes a difficult objective due to the strong interdependency between the variables involved and the existence of gravitational forces. Therefore the control methodology adopted must have the capability of coping with the stated difficulties.

The general form of the dynamics of a robotic manipulator is described by (41) where $M(q)$, $C(q,\dot{q})$, $g(q)$ and τ stand for the state varying inertia matrix, vector of Coriolis and centrifugal terms, gravitational forces and applied torque inputs, respectively. The nominal values of the plant parameters are given in Table 1 in standard units.

$$M(q)\ddot{q}+C(q,\dot{q})\dot{q}+g(q)=\tau \tag{41}$$

If the angular positions and angular velocities are described as the state variables of the system, six coupled and first order differential equations can define the model. In (42) through (45), the non-

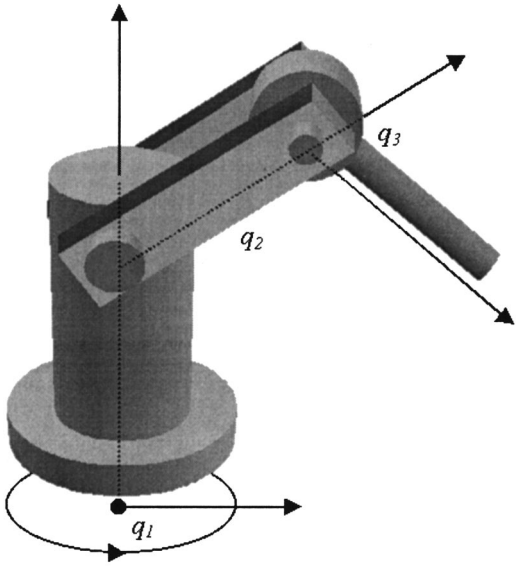

Fig. 7 Physical structure of the manipulator

Table 1 Manipulator parameters

Link 1 length	0.50	l_1
Link 2 length	0.40	l_2
Link 3 length	0.40	l_3
Link 1 mass	4.00	m_1
Link 2 mass	3.00	m_2
Link 3 mass	3.00	m_3
Distance link 1 CG-joint 1	0.20	l_{c1}
Distance link 2 CG-joint 2	0.20	l_{c2}
Cylindrical link radius	0.05	R
ith cylindrical link inertial parameter	$E_1=m_1R^2/2$, $E_i=m_i l_i^2/12$	E_i
ith cylindrical link inertial parameter	$A_i=m_iR^2/2$	A_i
ith cylindrical link inertial parameter	$I_i=m_i l_i^2/12$ for i=2,3	I_i
Link 1 torque limits	±50.00	$\tau_{sat\,1}$
Link 2 torque limits	±40.00	$\tau_{sat\,2}$
Link 3 torque limits	±20.00	$\tau_{sat\,3}$

zero entries of the state varying inertia matrix are described. The nonzero Cristoffel symbols are given in (46)–(49). The details of the plant model are presented in [18–19].

$$M_{11}=m_2l_{c2}^2\cos^2(q_2)+m_3(l_2\cos(q_2)+l_{c3}\cos(q_2+q_3))^2+E_1+A_2\sin^2(q_2)+E_2\cos^2(q_2)+A_3\sin^2(q_2+q_3)+E_3\cos^2(q_2+q_3) \quad (42)$$

$$M_{22}=m_2l_{c2}^2\sin^2(q_2)+m_3(l_2^2+l_{c3}^2+2l_2l_{c3}\cos(q_3))+I_2+I_3 \quad (43)$$

$$M_{23}=M_{32}=m_3(l_{c3}^2+l_{c3}l_2\cos(q_3))+I_3 \quad (44)$$

$$M_{33}=m_3l_{c3}+I_3 \quad (45)$$

$$hc_1=(-m_2l_{c2}^2+A_2-E_2)\cos(q_2)\sin(q_2)+(A_3-E_3)\cos(q_2+q_3)\sin(q_2+q_3)+m_3(l_2\cos(q_2)+l_{c3}\cos(q_2+q_3))(-l_2\sin(q_2)-l_{c3}\sin(q_2+q_3)) \quad (46)$$

$$hc_2=\sin(q_2+q_3)(-m_3l_{c3}l_2\cos(q_2)+(-m_3l_{c3}^2+A_3-E_3)\cos(q_2+q_3)) \quad (47)$$

$$hc_3=m_2l_{c2}^2\cos(q_2)\sin(q_2) \quad (48)$$

$$hc_4=-m_2l_2l_{c3}\sin(q_3) \quad (49)$$

Coriolis and centrifugal terms are formulated as follows.

$$C(q,\dot{q})=\begin{bmatrix} 2hc_1\dot{q}_1\dot{q}_2+2hc_2\dot{q}_1\dot{q}_3 \\ -hc_1\dot{q}_1^2+2hc_4(\dot{q}_2\dot{q}_3+\dot{q}_3^2)+hc_3\dot{q}_2^2 \\ -hc_2\dot{q}_1^2-hc_4\dot{q}_2^2 \end{bmatrix} \quad (50)$$

Lastly, the gravity terms are obtained as given in (51) where P represents the gravity constant.

$$g(q_1,q_2,q_3)=\begin{bmatrix} 0 \\ (m_2l_{c2}+m_3l_2)P\cos(q_2)+m_3l_{c3}P\cos(q_2+q_3) \\ m_3l_{c3}P\cos(q_2+q_3) \end{bmatrix} \quad (51)$$

5 Simulation Studies

In the simulation studies presented, the plant introduced in the fourth section is controlled by the proposed control scheme. The aim is to produce some torque signals such that the application of which results in the observation of a sliding motion in the phase space. As the controller, the architecture discussed in the second section is adopted. The structure of the control system is as illustrated in Fig. 2, in which the plant is in an ordinary feedback loop,

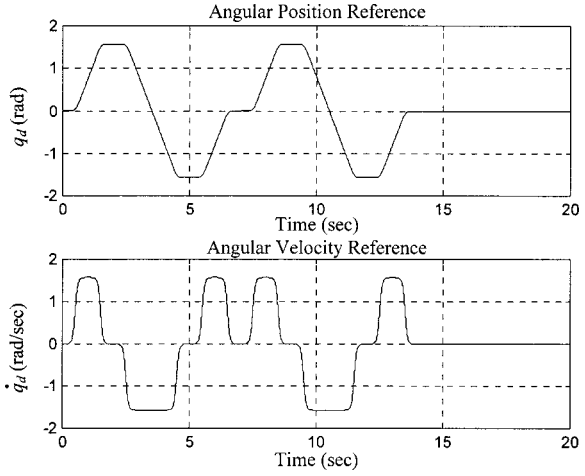

Fig. 8 Reference state trajectories

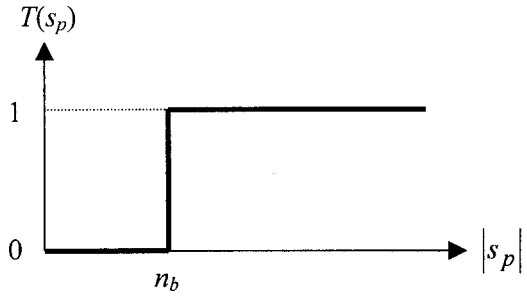

Fig. 9 Threshold function

to which the reference signal illustrated in Fig. 8 is applied for each link. Based on the tracking error vector, first the value of $s_p(e,\dot{e})$ is evaluated and this quantity is passed through the Ψ function to get the value of s_c, which is used in the dynamic adjustment mechanism. In evaluating the value of the quantity s_p, the slope parameter of the switching line (λ) has been set to unity for all three links.

In practical implementations of control structures for trajectory control of robotic manipulators, a number of difficulties are encountered, which make it difficult to achieve an accurate trajectory tracking. The simulation studies carried out address these difficulties. The first difficulty is the existence of gravitational forces adversely influencing the control performance. The second difficulty is the existence of observation noise. To study the effects of this situation, which is very likely to be encountered in practice, the information used by the controller is corrupted by a Gaussian distributed random noise having zero mean and variance equal to 0.33e-6. The peak magnitude of the noise signal is within $\pm$1e-3 with probability very close to unity. The third difficulty is the nonzero positional initial conditions. In order to demonstrate the reaching mode performance of the algorithm, the base link is moved to $\pi/18$ radians, the shoulder link is moved to $-\pi/18$ radians and the elbow link is moved to $\pi/18$ radians initially.

It should be pointed out that once the error or the rate of error comes very close to origin, the adjustment mechanism is driven solely by the noise sequence. Since the bound of perturbing signal is known, the dynamic equations of the parameters given in (29)–(31) can be modified so that a reduction on the unnecessary adjustment activity is obtained and the convergent behavior of the parameters can still be achieved by utilizing a sufficiently hard threshold function given by (52) and depicted in Fig. 9. The value of threshold is denoted by n_b and has been set to 5e-3 in the simulations. The equations of the controller parameters are therefore modified as given in (53)–(55).

$$T(s_p)=(1+\exp(-10^5(|s_p|-n_b)))^{-1} \quad (52)$$

$$\dot{G}_p=-\frac{e}{e^2+\dot{e}^2+1}k\,\text{sign}(\Psi(s_p))T(s_p) \quad (53)$$

$$\dot{G}_d=-\frac{\dot{e}}{e^2+\dot{e}^2+1}k\,\text{sign}(\Psi(s_p))T(s_p) \quad (54)$$

$$\dot{G}_c=-\frac{1}{e^2+\dot{e}^2+1}k\,\text{sign}(\Psi(s_p))T(s_p) \quad (55)$$

As the Ψ relation, the following selection is made parallel to the conditions discussed in the second section.

$$\Psi(x)=x \quad (56)$$

Furthermore, in order to reduce the chattering effect in the sliding mode, the function in (57) has been used instead of the sign function in the dynamic strategy described in (53)–(55).

$$\text{sign}(x)\approx\frac{x}{|x|+0.05} \quad (57)$$

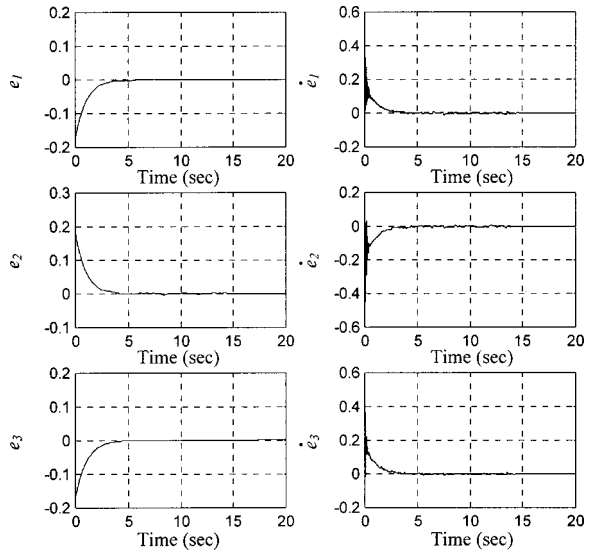

Fig. 10 State tracking errors

As the initial values for the controller parameters, the values given in (58) are adopted.

$$\begin{bmatrix} G_{p1}(0) & G_{p2}(0) & G_{p3}(0) \\ G_{d1}(0) & G_{d2}(0) & G_{d3}(0) \\ G_{c1}(0) & G_{c2}(0) & G_{c3}(0) \end{bmatrix} = \begin{bmatrix} -10 & -10 & -10 \\ -2 & -2 & -2 \\ 0 & 0 & 0 \end{bmatrix} \tag{58}$$

Under these conditions, the state tracking error graph in Fig. 10 is obtained. The trend in position and velocity errors clearly stipulate that the algorithm is able to achieve precise tracking objective with a sufficiently fast response. The motion in the phase plane is illustrated in Fig. 11. These figures show that after a fast reaching mode, a sliding mode is enforced and is maintained by producing a suitable control signal. In Fig. 12, the time behavior of the Lyapunov function in (38) is illustrated for each link. In order to

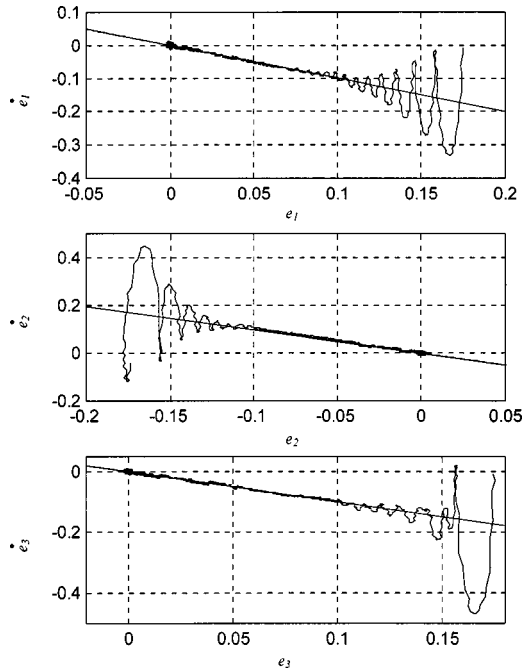

Fig. 11 Motion in the phase plane for each link

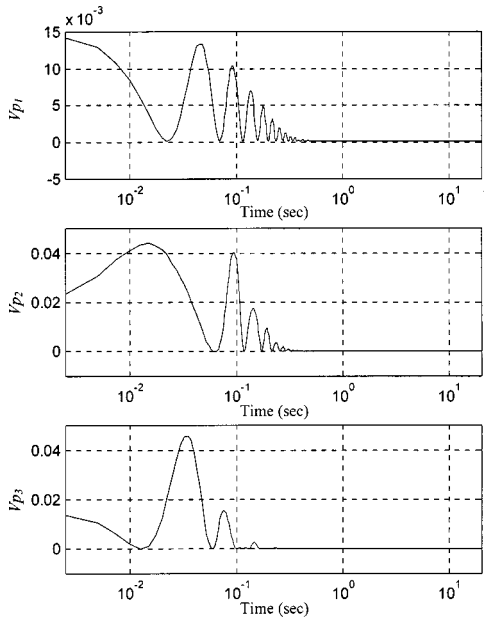

Fig. 12 Time behavior of the lyapunov function in (38) for each link

show the minimization activity of the algorithm presented, the horizontal axes of the subplots are selected as logarithmic. Clearly after $t=1$ s, the cost is almost zero, which means that the error vector lies in the vicinity of the sliding manifold. It is seen that some small magnitude spikes occur in time and they are dampened out quickly. We relate these spikes to the difficulties stated at the beginning of the section.

What should be emphasized as a last point is the smoothness of the torque signal produced by the controller. As seen in Fig. 13, the outputs of the shoulder and the elbow link controllers exceed slightly the limits of the applicable control ranges during the very early phase of the motion, during which a reaching mode is observed. Since the initial errors are considerably large in magnitude, evaluated torque signals (τ_e) are saturated and the applied torque signals (τ_a) are depicted in the right column of Fig. 13. However, the applied control signal has sufficiently smooth char-

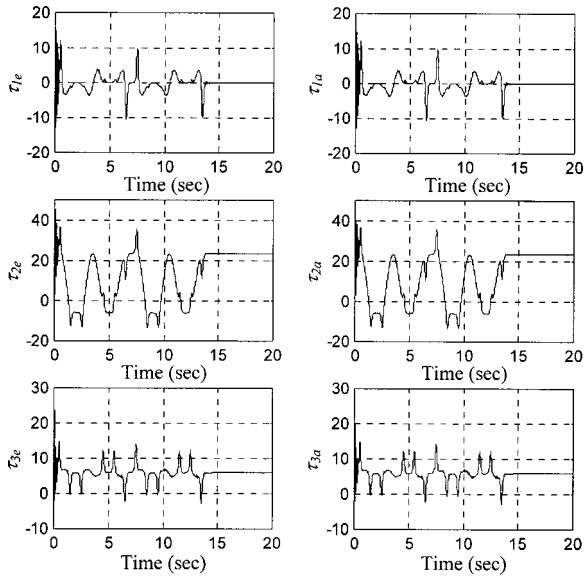

Fig. 13 Evaluated and applied torque inputs

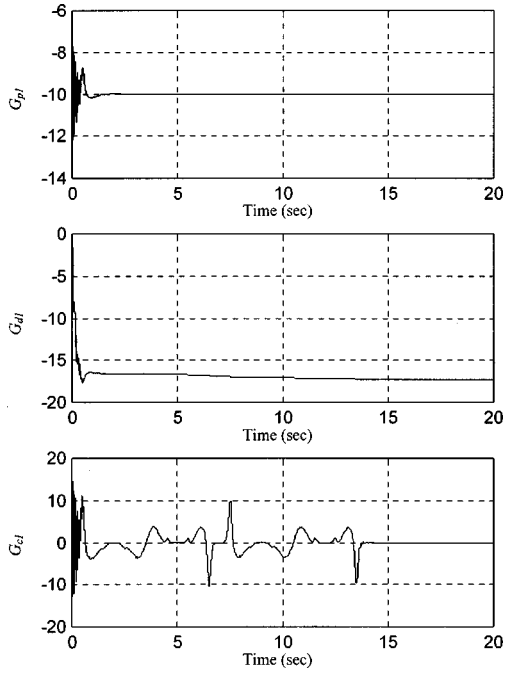

Fig. 14 Behavior of the parameters of the base link controller

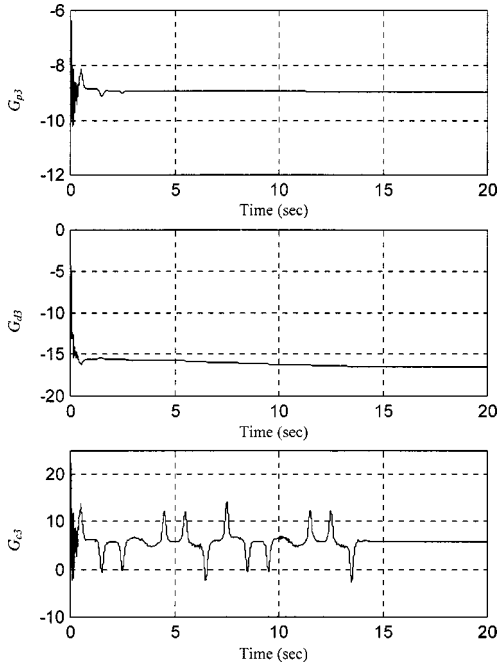

Fig. 16 Behavior of the parameters of the elbow link controller

acteristic, which does not violate the potential limits of the actuators. Lastly, the behavior of the controller parameters for base, shoulder and elbow links are illustrated in Fig. 14, Fig. 15, and Fig. 16, respectively. In these figures, it is seen that the parameters of the controllers remain bounded and are robust against the effect of noise around the origin of the phase space. Clearly, the threshold function ($T(s_p)$) of (52) introduces the elimination of the noise related evolution in the controller parameters.

During the simulations, the bounds for the uncertainties denoted by k for all three links has been set to 1000. The simulation stepsize has been selected as 2.5 ms and the time required to perform the simulation has been measured as 48 seconds on a Pentium II-233 PC running Matlab 5.1 software, indicating that the applicability of the algorithm in real-time.

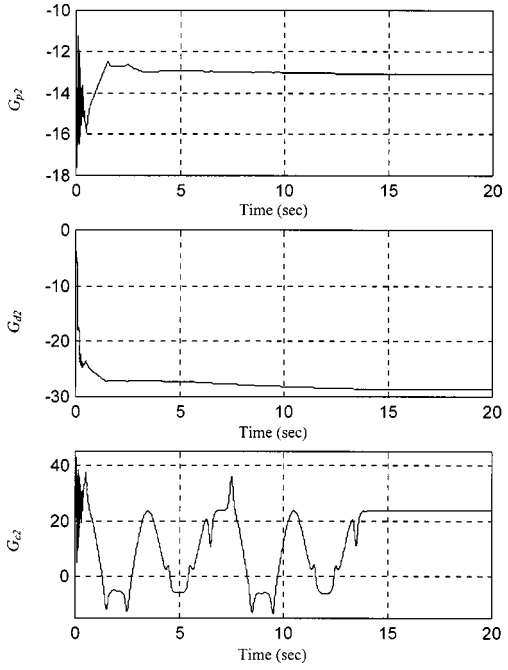

Fig. 15 Behavior of the parameters of the shoulder link controller

6 Conclusions

In this paper, a novel method for establishing a sliding motion in the dynamics of a three degrees of freedom anthropoid robot is discussed. The method is based on the adoption of a nonlinear dynamic adjustment strategy in an ADALINE based controller. The task is to drive the tracking error vector to the sliding manifold and keep it on the manifold forever. What makes the proposed algorithm so attractive in this sense is the fact that the sliding mode control of the plant is achieved while an equivalent regime is imposed on the controller parameters. In this way, the difficulties related to the noise on the measured quantities, gravitational forces and the structural uncertainties on the governing equations of the plant are alleviated by incorporating the robustness provided by the VSS technique into the proposed approach. A further attractiveness of the algorithm is the fact that the controller for each link possesses only three parameters. The computational requirement is not therefore excessive. From these points of view, the method proposed is highly promising in control engineering practice.

Acknowledgments

This work is supported by Bogazici University Research Fund (Project no: 99A202 and 00A203D) and TUBITAK (Project no: EEEAG-199E017).

References

[1] Emelyanov, S. V., 1967, *Variable Structure Control Systems*, Moscow, Nauka.
[2] Erbatur, K., Kaynak, O., Sabanovic, A., and Rudas, I., 1996, ''Fuzzy Adaptive Sliding Mode Control of a Direct Drive Robot,'' Rob. Auton. Syst., **19**, No. 2, pp. 215–227.
[3] Byungkook, Y., and Ham, W., 1998, ''Adaptive Fuzzy Sliding Mode Control of Nonlinear Systems,'' IEEE Trans. Fuzzy Syst., **6**, No. 2, pp. 315–321.
[4] Ertugrul, M., and Kaynak, O., 2000, ''Neuro Sliding Mode Control of Robotic Manipulators,'' Mechatronics, **10**, Nos. 1–2, pp. 243–267.
[5] Ertugrul, M., and Kaynak, O., 1998, ''Neural Computation of the Equivalent

Control in Sliding Mode For Robot Trajectory Control Applications,'' *Proc. of the 1998 IEEE Int. Conf. on Robotics and Automation*, Leuven, Belgium, pp. 2042–2047.
[6] Hung, J. Y., Gao, W., and Hung, J. C., 1993, ''Variable Structure Control: A Survey,'' IEEE Trans. Ind. Electron., **40**, No. 1, pp. 2–22.
[7] Gao, W., and Hung, J. C., 1993, ''Variable Structure Control of Nonlinear Systems: A New Approach,'' IEEE Trans. Ind. Electron., **40**, No. 1, pp. 45–55.
[8] Kaynak, O., Harashima, F., and Hashimoto, H., 1984, ''Variable Structure Systems Theory, as Applied to Sub-time Optimal Position Control with an Invariant Trajectory,'' Trans. IEE Jpn. Sec. E, **104**, Nos. 3/4, pp. 47–52.
[9] Bekiroglu, N., 1996, ''Adaptive Sliding Surface Design for Sliding Mode Control Systems,'' Ph.D. thesis, Bogazici University, Istanbul.
[10] Young, K. D., Utkin, V. I., and Ozguner, U., 1999, ''A Control Engineer's Guide to Sliding Mode Control,'' IEEE Trans. Control Syst. Technol., **7**, No. 3, pp. 328–342.
[11] Kaynak, O., and Denker, A., 1993, ''Discrete-Time Sliding Mode Control in the Presence of System Uncertainty,'' Int. J. Control, **57**, No. 5, pp. 1177–1189.
[12] Efe, M. O., and Kaynak, O., ''A Novel Optimization Procedure for Training of Fuzzy Inference Systems By Combining Variable Structure Systems Technique and Levenberg-Marquardt Algorithm,'' Fuzzy Sets Syst. (accepted for publication).
[13] Efe, M. O., and Kaynak, O., 2000, ''Stabilizing and Robustifying the Learning Mechanisms of Artificial Neural Networks in Control Engineering Applications,'' Int. J. Intell. Syst., **15**, No. 5, pp. 365–388.
[14] Efe, M. O., Kaynak, O., and Wilamowski, B. M., 2000, ''Stable Training of Computationally Intelligent Systems By Using Variable Structure Systems Technique,'' IEEE Trans. Ind. Electron., **47**, No. 2, pp. 487–496.
[15] Sira-Ramirez, H., and Colina-Morles, E., 1995, ''A Sliding Mode Strategy for Adaptive Learning in Adalines,'' IEEE Trans. Circuits Syst., I: Fundam. Theory Appl., **42**, No. 12, pp. 1001–1012.
[16] Yu, X., Zhihong, M., and Rahman, S. M. M., 1998, ''Adaptive Sliding Mode Approach for Learning in a Feedforward Neural Network,'' Neural Comput. Appl., **7**, pp. 289–294.
[17] Slotine, J.-J. E., and Li, W., 1991, *Applied Nonlinear Control*, Prentice-Hall, Englewood Cliffs, NJ.
[18] Erbatur, K., Vinter, R. B., and Kaynak, O., 1994, ''Feedback Linearization Control for a 3-DOF Flexible Joint Elbow Manipulator,'' *Proc. 1994 IEEE Int. Conference on Robotics and Automation*, Vol. 4, pp. 2979–2984, San Diego.
[19] Stadler, W., 1995, *Analytical Robotics and Mechatronics*, McGraw-Hill, New York, p. 476.